



## Structural and impedance characterization of ceramics prepared from NPK fertilizer

Diouma Kobor\*, Ousmane Bodian, Waly Bodian, Abdou Kadri Diallo, Modou Tine

*Laboratoire de Chimie et de Physique des Matériaux (LCPM), Département de Physique, University Assane Seck of Ziguinchor, Ziguinchor, Senegal*

Received 25 April 2015; Received in revised form 6 June 2015; Received in revised form 21 June 2015;  
Accepted 27 June 2015

### Abstract

*One of the main objectives of this work was to study the possibilities of valorising the phosphates through the development of a conductive ceramics using NPK fertilizer as a precursor. Phosphorus based powders were synthesized using solid state technique from NPK fertilizer, lithium chloride and iron chloride at different temperatures up to 900 °C and ceramic samples were prepared by the powder pressing and sintering at 1100 °C. XRD spectra of the calcined powders show various sharp peaks indicating a relatively high degree of crystallinity and presence of different crystalline phases, such as: phosphorus based crystalline compounds ( $AlPO_4$  and  $LiFePO_4$ ), ferrite ( $Fe_3O_4$  and  $DyFeO_3$ ),  $CaSO_4$  and  $K_3DyCl_6$ . The prepared phosphorus based ceramics showed very interesting electrical and dielectric properties. Thus, in the future the obtained ceramics could find application in electronic or energy storage devices. However, further investigations are necessary to understand the exact chemical composition and structural characteristics of this material, to better understand the origin of the obtained electrical and dielectric behaviour.*

**Keywords:** *phosphorus based ceramics, structural characterization, electrical and dielectric properties*

### I. Introduction

Studies on lithium iron phosphates have been greatly stimulated by applying these materials as cathodes in the next generation of Li-ion rechargeable batteries. The interest in these systems started with the discovery of lithium excellent intercalation performance in  $LiFePO_4$  with the olivine structure [1]. Besides its obvious advantages like: high capacity, low production costs and environmental friendliness, crystalline  $LiFePO_4$  phosphor-olivines have a serious drawback: a low electrical conductivity (reported values spread from  $10^{-10}$  S/cm [2] to  $10^{-7}$  S/cm [3] at room temperature). Most researchers have circumvented the problem of low conductivity of  $LiFePO_4$  by preparing composites of the parent lithium phosphor-olivine materials with carbon. Nevertheless, several authors have recently proposed and studied alternative ideas of conductivity enhancement. Ceder *et al.* [4] used nonstoichiometric olivine-like materials (i.e.,  $LiFe_{0.9}P_{0.95}O_{4.6}$ ) to prepare cathodes in lithium

batteries that could operate at very high current rates.

The use of photovoltaic (PV) on a larger scale is hampered by the high cost of these energy conservation devices available during the day and unavailable at night. People in developing countries do not have access to this energy source because of the lack of operating resources. To conserve this energy, lithium-iron-phosphate batteries (LFP) seem to be currently the best. Unfortunately, costs are still high and are often as expensive as PV modules. A goal was set to find materials that reduce both the manufacturing cost and the price of products used in the manufacture of these batteries through the use of accessible precursors and at very low cost. The NPK fertilizer, being predominantly made up of phosphorus and some harmless lithium family ions (K), seems to be one of the best possibilities. Developing ceramics using this fertilizer, which is largely available in Senegal, allow the researchers to try and optimize manufacturing conditions. Then, studies on the structural, chemical, thermal [5], electrical and dielectric properties were conducted. The objective of this work is to study the structural, conduction, dielectric

\*Corresponding author: tel: +221 77 9166518,  
fax: +221 33 9916809, e-mail: dkobor@univ-zig.sn

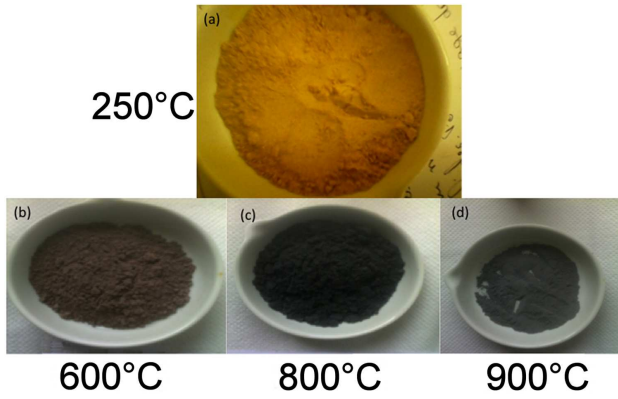


Figure 1. The synthesized powders calcined at: a) 250 °C, b) 600 °C, c) 800 °C and d) 900 °C

properties and capacity nonlinearity of ceramics prepared from the powders synthesized at different calcination temperatures.

## II. Experimental procedure

In this section, synthesis of a phosphorus based ceramics from NPK fertilizer, lithium chloride and iron chloride is described. The structural and electrical characterizations of the obtained materials at different temperatures are also discussed.

### 2.1. Synthesis

NPK fertilizer, LiCl (99%) and  $\text{FeCl}_3 \times 6\text{H}_2\text{O}$  (99%) were used as starting materials. The NPK fertilizer contains ~23 wt.% of phosphor and a non-negligible quantity of Al, K, Ca and N (Table 1) considered here as dopants. The phosphorus based ceramics were synthesized using the solid state technique and Li/Fe/ $\text{PO}_4$  molar ratio of 1 : 1 : 1/2, as described in our previous paper [5]. Powders were mixed in alcohol, dried and finally calcined at 600, 800 and 900 °C for 2 hours (Fig. 1) using a muffle furnace K114 of GmBH. The resulting powders were mixed with 10 wt.% polyvinyl alcohol (PVA) solution and uniaxial pressed at 80 MPa to prepare pellets with the diameter of 13 mm and thickness of 1.2 mm. The pellets were sintered at 1100 °C for 4 hours in a sealed crucible.

### 2.2. Structural analysis

X-ray powder diffraction was performed to the calcined powder on a D8 Advance Bruker AXS diffractometer equipped with a Rapid Vantec-1 detector using a monochromatic selecting  $\text{CuK}\alpha$  radiation ( $\lambda = 1.5418 \text{ \AA}$ ). For this sample the diffractometer is in theta-theta configuration (the X-ray source and the detector move while the sample remains stationary).

### 2.3. Electrical measurement

The electrical conductivity ( $\sigma$ ) is a property that varies extremely with the materials type, its exact chemistry, microstructure and purity. To study the electrical properties, both surfaces of the sintered pellet were

metallized with silver paste using the screen printing method. In order to have good adhesion between the metal and the ceramic, the metallized sample was annealed at 400 °C for 30 min. For this characterization technique, a sample was mounted in a series circuit with a direct current generator. Sample DC conductivity was deduced from its geometric parameters and resistance by the following equation (at low frequencies):

$$R_e = \frac{l}{\sigma \cdot S} \quad (1)$$

where  $l$  is the thickness,  $S$  the surface and  $\sigma$  the electrical conductivity of a sample.

For AC conductivity measurements, impedance was determined using an oscilloscope which measures the current and phase shift by varying the frequency. Figure 2 shows the electrical circuit for measurement. Resistance ( $R = 500 \text{ k}\Omega$ ) was used to measure the current through the sample  $I = V_r/R$ , probe-1 ( $V_e$ ) was used to measure the voltage applied to the sample and probe-2 ( $V_r$ ) was used to measure the voltage applied to the resistance. The impedance was calculated from the following formula:  $Z_e = R \cdot V_e/V_r$ . The phase difference  $\phi$  between the two signals was taken from the resultant Lissajous figure, and that for each frequency of 1 kHz to 500 kHz. The complex impedance ( $Z$ ) consists of real ( $Z'$ ) and imaginary part ( $Z''$ ) which are related as  $Z = Z' - jZ''$  and calculated using  $Z' = Z_e \cos \phi$  and  $Z'' = Z_e \sin \phi$ . Measuring and calculating these values at various temperatures, one can determine the AC conductivity  $\sigma_{AC}$  with the following equation:

$$\sigma_{AC} = \frac{1}{S} \frac{Z'}{Z'^2 + Z''^2} \quad (2)$$

The frequency dependent properties of a material can also be described as complex permittivity ( $\epsilon^*$ ) and dielectric loss or dissipation factor ( $\tan \delta$ ). The real ( $\epsilon'$ ) and imaginary ( $\epsilon''$ ) parts are in turn related to one another as  $\epsilon^* = \epsilon' + j\epsilon''$ . These parameters are related to the real and imaginary parts of the impedance as follows:

$$\epsilon' = -\frac{Z''}{\omega \cdot C_0 (Z'^2 + Z''^2)} \quad (3)$$

Table 1. Chemical composition of NPK fertilizer

Elements	Content [wt.%]
N	9.00
P	23.00
K	30.00
( $\text{Al}_2\text{O}_3 + \text{Fe}_2\text{O}_3$ )	5.00 – 17.00
Ca	1.50
Mg	0.6
Si	3.00 – 30.00
F	1.60 – 2.00
Cl	0.04 – 1.01

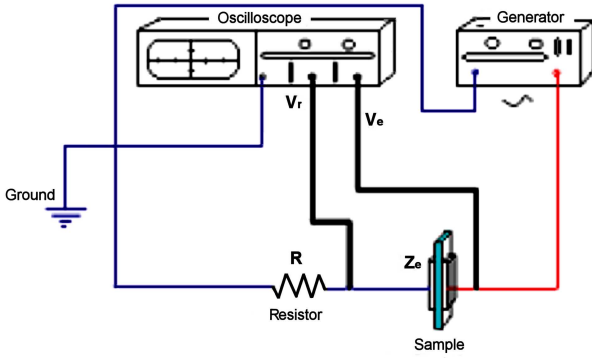


Figure 2. Impedance electrical measurement circuit

$$\epsilon'' = -\frac{Z'}{\omega \cdot C_0 (Z'^2 + Z''^2)} \quad (4)$$

$$\tan \delta = \frac{\epsilon''}{\epsilon'} \quad (5)$$

The ceramic capacity  $C_e$  was deduced from the plot of the logarithm of  $\text{Im}(Z)$  versus the logarithm of the sample frequency ( $f_e$ ) using the following relation:

$$-\ln C_e - \ln 2\pi = V_0 \quad (6)$$

where  $V_0$  is value at intercept 0. The relative dielectric permittivity  $\epsilon_r$  was calculated after the determination of capacity  $C_e$  value at different temperatures.

The standard capacitor in use throughout the world in electronic circuits today is supposed to be a linear device that follows the formula below:  $Q = C \cdot V$ . Very simply,  $Q$  is the number of electrons that come out of the capacitor with the application of a voltage (positive voltage equals positive  $Q$ ). In a linear capacitor, this number of electrons is exactly proportional to the applied voltage ( $V$ ) and the capacitance ( $C$ ). In a linear capacitor,  $C$  is a constant of proportionality independent of voltage. If a triangle wave is applied to this linear capacitor and electrons that exit from and enter in the capacitor are counted manually as the voltage signal application, a perfect line could be obtained. Counting the electrons versus voltage is the fundamental operation performed by research-level ferroelectric testers. Some capacitors have a non-linear response to voltage, making them interesting devices to apply to memories, pressure sensors, heat sensors and other useful activities. Most capacitors with this property are called ferroelectric capacitors. Other non-linear types are paraelectric capacitors and electret capacitors. In this experiment, a simple circuit was constructed for ferroelectric hysteresis measurement using a function generator and an oscilloscope. This approach was first used by Sawyer and Tower [4] in 1929 to measure one of the earliest known ferroelectric materials, Rochelle salt. It was well known at the time that two capacitors in series share charge when a voltage is applied across the stack. Sawyer and Tower used the capacitance of the deflection plates of the early oscilloscope in series with a Rochelle salt ca-

pacitor to see the hysteresis loop [6]. Rochelle salt will be replaced by our ceramic sample as capacitor. The amount of charge generated by the ferroelectric capacitor can be determined by multiplying the measured voltages on the oscilloscope by the size of the sense capacitor, 100 nF. The polarization can then be found by dividing the calculated charge by the area of the capacitor, 1.54 cm<sup>2</sup>.

### III. Results and discussion

#### 3.1. Structural analysis

Figure 3 shows X-ray diffraction patterns of the samples synthesized by solid state reactions at 600, 800 and 900 °C. The presence of various sharp peaks indicates a relatively high degree of crystallinity and different crystalline phases might be identified, such as: phosphorus based crystalline compounds ( $\text{AlPO}_4$  and  $\text{LiFePO}_4$ ), ferrite ( $\text{Fe}_3\text{O}_4$  and  $\text{DyFeO}_3$ ),  $\text{CaSO}_4$  and  $\text{K}_3\text{DyCl}_6$ . Thus, the presence of some peaks at 21°, 26° and 37° indicates the possible presence of  $\text{LiFePO}_4$  and  $\text{Fe}_3\text{O}_4$  components [7]. In addition, the characteristic peaks at 23 and 28° on one side and those at 34, 48 and 54° on the other could be due to the presence of  $\text{AlPO}_4$  and  $\text{DyFeO}_3$ , respectively. The appearance and disappearance of some peaks as a function of the heating temperature were also noticed. The doublet peak which appears at 17° in the spectra of the samples calcined at 800 and 900 °C (Figs. 3b and 3c) does not exist in the XRD pattern of the powder synthesized at 600 °C (Fig. 3a). At the same time, peaks observed at 20 and 69° appear only in the spectrum of the sample calcined at 600 °C. The shape and intensity of some peaks also change showing a new structure or crystalline phases and the prevalence or disappearance of certain elements. Note also that the most intense peak in the sample calcined at 600 °C is detected at 27° while those are between 30 and 37° for the samples calcined at higher temperatures. Finally, it can be said that the ceramic synthesized at 600 °C does not have the same crystalline phases as those calcined at 800 and 900 °C, which are almost the same.

The results from EDX analysis made for the sample calcined at 900 °C (Fig. 4) are consistent with the fact that the ceramic is composed of calcium-phospho-alumino-sulfate based components, with Li, K, Fe and Dy as substituting atoms. The aluminum peak is the sharpest indicating the presence higher amount of aluminum-based compounds.

#### 3.2. Electrical measurement

Figure 5 shows the ceramic resistance variation as a function of temperature from 40 to 120 °C. A linear dependence of the logarithm of resistance versus inverse temperature can be observed. This change in resistance as a function of temperature is also characteristic of NTC (negative temperature coefficient) thermistors [7]. These NTC are mainly oxides semiconductors. The relationship between resistance and temperature for such

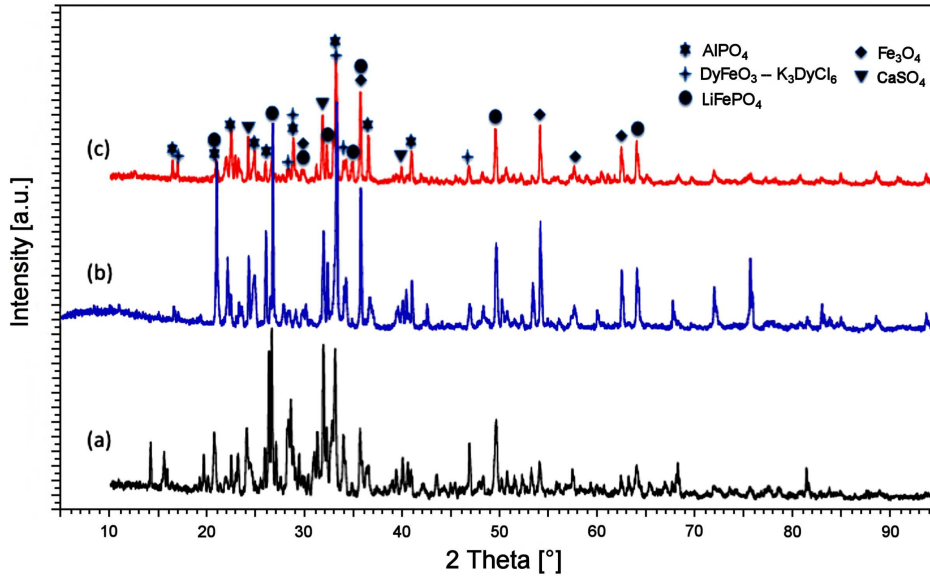


Figure 3. X-ray powder diffraction patterns of samples calcined at: a) 600 °C, a) 800 °C and a) 900 °C

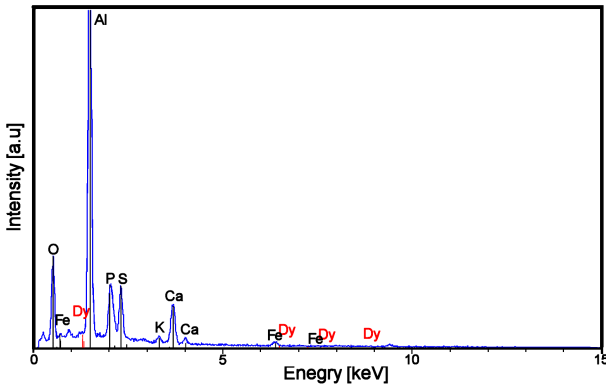


Figure 4. EDX spectrum of the sample calcined at 900 °C

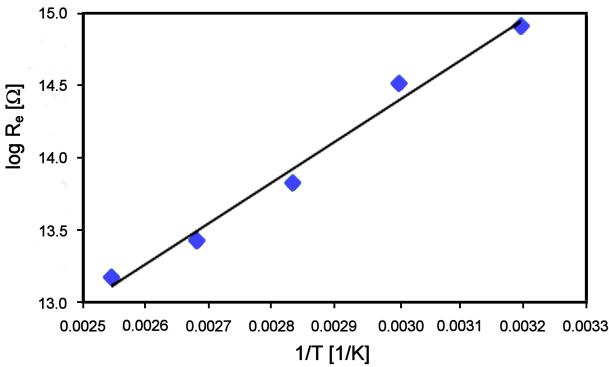


Figure 5. The resistance variation measurement according to temperature

materials is expressed by equation 7:

$$R(T) = R(T_N) \cdot \exp\left[\beta\left(\frac{1}{T} - \frac{1}{T_N}\right)\right] \quad (7)$$

where  $R(T)$  is resistance at temperature  $T$ ,  $R(T_N)$  resistance at known temperature  $T_N$  and  $\beta$  a characteristic constant of the thermistor that indicates the relationship of material resistivity to temperature. From Eq. 7,  $\beta$  can be derived and the sensitivity of the thermistor defined by the temperature coefficient of resistance ( $\alpha$ ), which can be expressed as a function of  $\beta$  parameter according to the following equation [8–10]:

$$\alpha = \frac{1}{R} \frac{dR}{dT} = -\frac{\beta}{T^2} \quad (8)$$

From the plot presented in Fig. 5,  $\beta$  was calculated in the temperature range from 313 to 393 K and is equal to 2798.5 K. The  $\alpha$  parameter at 313 and 393 K is equal to -2.86 and -1.81%.K<sup>-1</sup>, respectively (Table 2). These values are consistent with those found for good quality thermistors generally having  $\beta$  between 2000 and 4000 K.

Figures 6,7 and 8 show the variation of  $\sigma_{AC}$  with frequency at different temperatures (40, 60, 80, 100 and 120 °C) for the ceramic prepared from the powder synthesized at 900 °C. Figure 6 represents a relation between  $\sigma_{AC}$  and the logarithm of frequency ( $\log f_e$ ). One can identify three frequency regions: the low fre-

Table 2. Electrical conductivity parameters of the synthesized ceramic at different temperatures

$T$ [K]	$n$	$A$ [S/(cm·rad·s)] ( $10^{-12}$ )	$\epsilon_r$	$C$ [pF]	$\alpha$ [%/K]
313	0.97	1.04	31	43	-2.86
333	0.65	51.21	70	95	-2.52
353	0.51	361.77	471	642	-2.25
373	0.46	1071.70	818	1115	-2.01
393	0.36	4465	3223	4391	-1.81

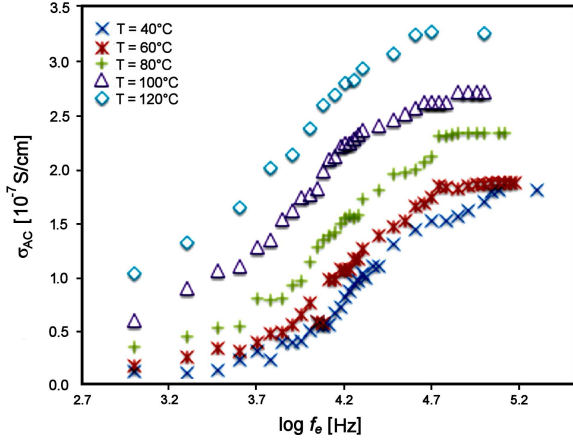


Figure 6. AC conductivity versus the frequency logarithm at temperature range from 40 to 120 °C

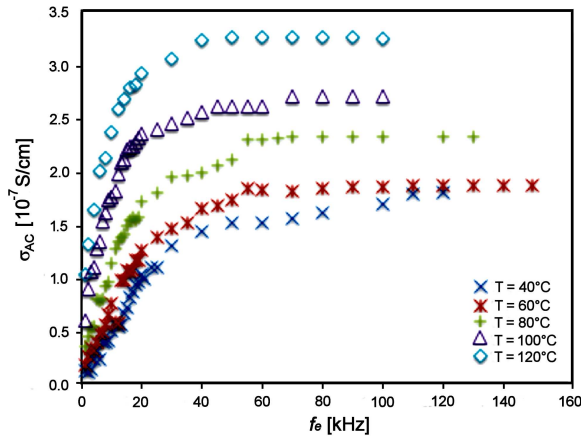


Figure 7. AC conductivity versus the frequency at temperature range from 40 to 120 °C

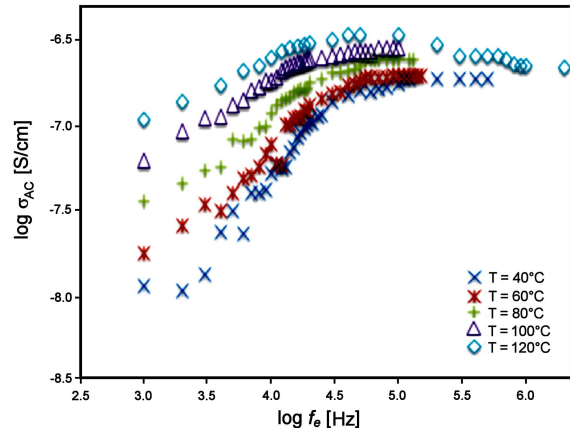


Figure 8. AC conductivity versus the frequency at temperature range from 40 to 120 °C

frequencies region, in which, the value of  $\sigma_{AC}$  is almost the  $\log f_e$  independent, but is temperature dependent. In the second region, the conductivity depends on both the temperature and  $\log f_e$ . The linear variation of  $\sigma_{AC}$  with the  $\log f_e$  proves that a  $\log \omega$  term should exist in the conductivity expression. Finally, in the third region (high frequencies), we find the same behaviour as in low

frequencies, i.e. the conductivity depends only on the temperature, but not on the  $\log f_e$ .

Figure 7 presents the relation between  $\sigma_{AC}$  and the frequency. It shows that the conductivity depends on both temperature and frequency in the low frequency region ( $<20$  kHz) while it is non-frequency dependence in the high frequency region ( $>20$  kHz). The imaginary parts tend to zero and the ceramic has the same behaviour as a resistor ( $\text{Im}(Z) = 0$  at very high frequencies  $>100$  kHz). Its appearance suggests the existence of an  $\omega$  power term ( $\omega^n$ ) in  $\sigma_{AC}$  expression. Figure 8 shows, the double logarithmic plot, i.e.  $\log \sigma_{AC}$  vs  $\log f_e$ . These curves show two regions. One in which a linear dependence of  $\log \sigma_{AC}$  to  $\log f_e$  exists and the high frequency region, where all logarithmic values tend towards a constant. The graphs are characterized by the universal dynamic response (the power law, Eq. 9 [11,12]):

$$\sigma_{AC}(\omega) = A \cdot \omega^n \quad (9)$$

The slope of each line gives the value of the frequency exponent  $n$  at the corresponding temperature:

$$n = \frac{\Delta \ln \sigma_{AC}}{\Delta \ln \omega} \quad (10)$$

The value of the constant  $A$  can be obtained by plotting  $\log \sigma_{AC}$  versus  $\log \omega$ , with  $\omega = 2\pi f_e$ . The values of  $n$  and  $A$  are summarized in Table 2.

Regarding the conduction mechanism, it is known that, there are three distinct processes [13] that have been proposed; namely, quantum mechanical tunnelling (QMT) through the barrier, classical hopping over the barrier (CBH) and small polaron tunnelling (SPT). The expression for AC conductivity due to (QMT) is given by [14]:

$$\sigma(\omega) = \frac{\eta}{3} l^2 kT [N(E_f) \cdot T]^2 \alpha^{-5} \omega \left[ \ln \left( \frac{\nu_{ph}}{\omega} \right) \right]^4 \quad (11)$$

where  $N(E_f)$  is the density of states at Fermi level,  $\nu_{ph}$  is the phonon frequency in the order of  $10^{13} \text{ S}^{-1}$  and  $\alpha$  is the decay of the localized states wave function ( $\alpha = 1 \text{ \AA}$ ) [15]. The expression that describes the behaviour of  $n$ , in the QMT model is given by:

$$n = 1 - \frac{4}{\ln \frac{\nu_{ph}}{\omega}} \quad (12)$$

whereas, for classical hopping:

$$n = 1 - \frac{6kT}{E_0 - kT \ln \frac{\nu_{ph}}{\omega}} = 1 - \frac{6kT}{E_0 - kT \ln \frac{1}{\omega\tau}} \quad (13)$$

and for small polaron [15]:

$$n = 1 - \frac{4}{\ln \frac{1}{\omega\tau} - \frac{W_H}{kT}} \quad (14)$$

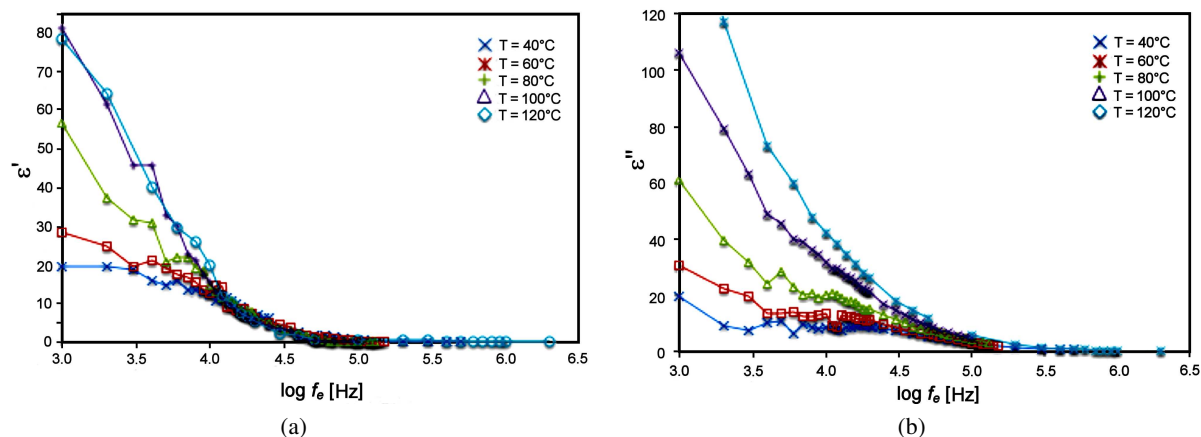


**Figure 9.** The dielectric permittivity real (a) and imaginary part (b) versus the logarithm of the frequency at different temperatures

The symbols take their usual meanings.  $k$  is Boltzmann's constant,  $T$  is absolute temperature,  $E_0$  is optical energy gap,  $\omega$  is angular frequency,  $\nu_{ph}$  and  $\tau$  ( $\tau = 1/\nu_{ph}$ ) are the phonon frequency and the relaxation time, respectively, and  $W_H$  is the activation energy involved to the electron transfer process between a pair. From Eqs. 11 and 12 for QMT model, it is clear that the value of  $n$  is temperature independent whereas, for hopping model, Eq. 13, the value of  $n$  decreases with increasing temperature and less dependent on the frequency, and finally, Eq. 14 predict that  $n$  increases as  $T$  increases. Table 2 indicates that the value of  $n$  decreases with increasing temperature.

This means that, in the investigated temperature region, the data could indicate on the hopping model (CBH) conduction. The values of activation energy at low and high frequency regions are determined by plotting the Arrhenius curve. The value of 0.30 eV was found for the low frequency region while in high frequency region the corresponding value is 0.08 eV. The first value was previously reported by Hong *et al.* [16,17] which they assigned to the hopping process induced by oxygen vacancy. The activation energy of 0.30 eV can also indicate that the grain boundaries are trap-controlled and reveal the heterogeneity of grain distribution and of grain boundaries (grain boundary relaxation activation energy). The activation energy of 0.08 eV is very near to 0.1 eV which is associated with an oxygen interstitials  $O_i^{1+}$  and  $O_i^0$  [18,19] so, close to the value of the first ionization energy of the oxygen vacancy ( $V_O^{\bullet\bullet}$ ) or grain relaxation. This value is the same as the activation energy found in n-type semiconductors.

Table 2 shows an increasing of  $A$  as the temperature increases which means the polarizability increases as temperature increases. Figure 9 plots the frequency dependence of real ( $\epsilon'$ ) and imaginary ( $\epsilon''$ ) dielectric constant at various temperatures of the ceramics prepared from the powder synthesized at 900 °C. It is observed from Fig. 9a that the dielectric permittivity sharply decreases with increasing frequency (<100 kHz), and the

rate of decrease levels off in a certain frequency range (>100 kHz). At a relatively low frequency, the dielectric permittivity strongly depends on frequency, evidently showing a dielectric dispersion [20]. Such a strong dispersion seems to be a common feature in dielectric materials concerned with ionic conductivity, which is referred to as low-frequency dielectric dispersion. When the frequency increases, the relative effect of ionic conductivity becomes small and as a result, the frequency dependence of the dielectric constant becomes weak. At lower frequencies, the dipolar complexes will be able to keep up with the applied field and reorient with each half cycle. The full effect of the polarization reversal will contribute to the dielectric constant [21]. Figure 9b represents the frequency dependence of imaginary dielectric permittivity  $\epsilon''$  at various temperatures. Similar to the behaviour of dielectric permittivity with frequency, the dielectric loss increases with increasing temperature. No loss peak was observed in the  $\epsilon''$  spectra. The high values of  $\epsilon''$  at high temperatures and the large drop of  $\epsilon''$  with an increase in frequency seem to indicate the influence of conductivity and space charge polarization. This indicates the thermally activated nature of the dielectric relaxation of the system. The fast rising trend of  $\epsilon''$  at low frequencies may be due to the polarization mechanism associated with the thermally activated conduction of mobile ions and/or other defects [22]. High values of dielectric permittivity are observed only at high temperatures and very low frequencies, which may be due to the free charge build up at interfaces within the bulk of the sample (interfacial Maxwell-Wagner polarization) [23] and at the interface between the sample and the electrodes (space-charge polarization).

Figure 10 illustrates imaginary part  $\epsilon''$  versus real part  $\epsilon'$  of the permittivity of the ceramic at various temperatures and different frequencies (from 1 kHz to 500 kHz). The figure indicates a polydispersive nature of dielectric phenomenon in the ceramic with distributed relaxation time as indicated by the presence of semicircular arcs at different temperatures with

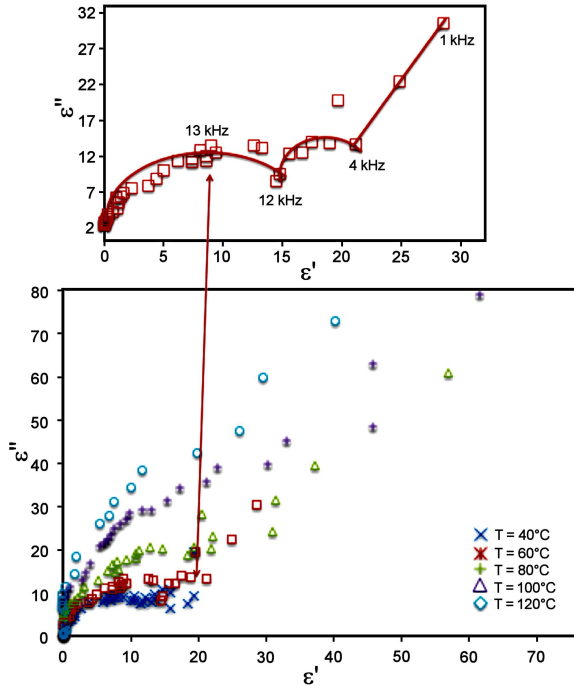


Figure 10. The dielectric permittivity Cole-Cole plot of the ceramic at different temperatures

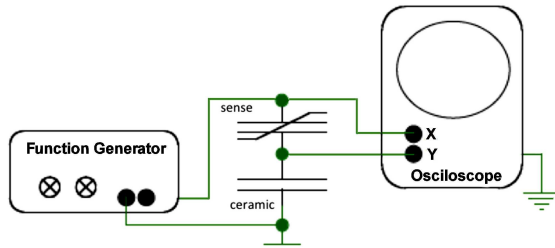


Figure 11. Modern Sawyer-Tower circuit

their center located below the real permittivity axis  $\epsilon'$ . Clearly the Cole-Cole plot indicates that dielectric phenomenon is different from Debye type mono dispersive phenomenon [24].

They are also characterized by the appearance of another semicircular spur and the existence of a linear por-

tion in the low-frequency range, which makes an angle of about  $45^\circ$  to the real permittivity axis, which may be attributed possibly to the diffusion phenomenon of Warburg type arising due to ion migration [25]. This kind of behaviour (the Warburg diffusion) is typical of compounds with ionic conductance and typical of ceramics having conductive grain boundary arising out of a relaxation process of the Maxwell-Wagner type. The relatively high values of the relative dielectric permittivity of the ceramic (31 to 3223 for 40 to 120 °C, respectively - Table 2) confirm that it can be a ferroelectric material. So it was important to investigate this property too.

The circuit in Fig. 11 that we built is the one of the modern version of the Sawyer-Tower measurement apparatus using a linear capacitor as the sense circuit. The function generator applies an alternating voltage across the capacitor stack, forcing charge onto the top plate of the ferroelectric capacitor. The same amount of charge will be forced to leave the opposite plate of the ferroelectric capacitor and be collected on the top plate of the linear sense capacitor. According to the equation “ $Q = CV$ ”, the voltage across the linear sense capacitor will thus represent the number of electrons that move into or out of the ferroelectric capacitor as a result of the applied waveform. Channel 2 of the oscilloscope will capture this voltage while Channel 1 captures the voltage applied by the function generator. Placing the oscilloscope in the X : Y graphing mode will allow us to see the hysteresis loop. The function generator is driving a 9 V 100 Hz sine wave. Figure 12a shows the stimulus and the response signals as a function of time. The stimulus triangle wave (X) and the voltage (sine wave) across the sense capacitor (Y) prompt the consideration that the ceramic has a ferroelectric behaviour. The ceramic capacitor is modulating the stimulus wave. The modulation by the ferroelectric capacitor is particularly apparent in Fig. 12b. This figure presents a ferroelectric hysteresis loop by using X : Y mode as explained in the experimental method. This hysteresis confirms that the ceramic prepared from the powder synthesized at 900 °C might have a ferroelectric behaviour. It seems that the values of remnant polariza-

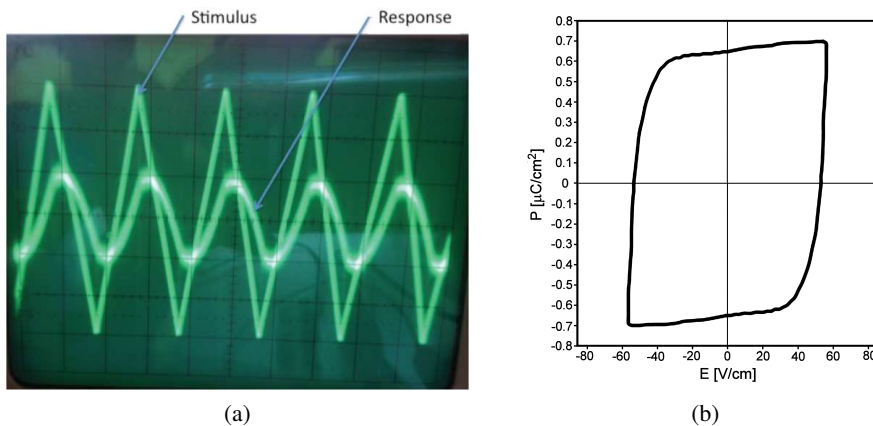


Figure 12. Modulation of the stimulus triangle wave (a) and its hysteresis loop (b)

tion  $P_r$  and spontaneous polarization  $P_s$  are equal to  $0.65 \mu\text{C}/\text{cm}^2$  and  $0.70 \mu\text{C}/\text{cm}^2$ , respectively. The ferroelectric behaviour could be explained by the XRD and the EDX (Figs. 3 and 4) results that demonstrated the presence of different crystalline phases. Among them  $\text{AlPO}_4$  is known as a piezoelectric material but non-ferroelectric, thus, there are two possible explanations for the ferroelectric behaviour of the material. The ferroelectricity behaviour may come from the presence of ferrite ( $\text{DyFeO}_3$ ) or some other perovskite or tetragonal tungsten bronze (TTB) phase. The presence of  $\text{DyFeO}_3$  was confirmed by the XRD analysis (Fig. 3), but due to a lot of diffraction peaks (Fig. 3) it was not possible to confirm the presence of some other phases, which might show ferroelectric behaviour. Thus, further investigations are necessary to understand the exact chemical composition and structural characteristics of this material and to the origin of the observed behaviour.

#### IV. Conclusions

In this paper, we present the synthesis, physico-chemical and electrical characterization of ceramics fabricated using NPK fertilizer as phosphorus precursors. In the first step, the phosphorus based powders were synthesized using the solid state technique from NPK fertilizer, lithium chloride and iron chloride at different temperatures ( $600^\circ\text{C}$ ,  $800^\circ\text{C}$  and  $900^\circ\text{C}$ ). XRD spectra of the calcined powders show various sharp peaks indicating a relatively high degree of crystallinity and presence of different crystalline phases, such as: phosphorus based crystalline compounds ( $\text{AlPO}_4$  and  $\text{LiFePO}_4$ ), ferrite ( $\text{Fe}_3\text{O}_4$  and  $\text{DyFeO}_3$ ),  $\text{CaSO}_4$  and  $\text{K}_3\text{DyCl}_6$ . From these structural studies, the powder synthesized at  $900^\circ\text{C}$  was chosen and uniaxially pressed and sintered at  $1100^\circ\text{C}$ . The obtained ceramics were used for electrical measurements. Using the resistance versus temperature plot,  $\beta$  was calculated in the temperature range from 313 to 393 K and it is equal to 2798.5 K. The  $\alpha$  parameter at 313 and 393 K is equal to  $-2.86$  and  $-1.81\% \cdot \text{K}^{-1}$  respectively. The ceramic conductivity varies with the frequency following the universal dynamic response (UDR). In the investigated temperature region, the data confirm the classical hopping model (CBH) conduction and the activation energy in low and high frequency regions are equal to 0.30 eV and 0.08 eV, respectively. The dielectric permittivity study shows the Warburg diffusion behaviour, typical of compounds with ionic conductance and ceramics having conductive grain boundary arising out of a relaxation process of the Maxwell-Wagner type. The relative important value of the relative dielectric permittivity permits us to investigate the nonlinearity of the ceramic capacity using a Sawyer-Tower modern circuit. The shape of hysteresis loop indicates that the sintered ceramics might have a ferroelectric behaviour with the remnant polarization  $P_r$  and spontaneous polarization  $P_s$  equal to  $0.65 \mu\text{C}/\text{cm}^2$  and  $0.70 \mu\text{C}/\text{cm}^2$ , respectively.

**Acknowledgements:** Financial support of the Senegalese Ministry High Education and Research and the Economic Organization of West African Economic Monetary Union (WAEMU).

#### References

1. A. Aimable, D. Aymes, H. Muhr, C. Gentric, F. Bernard, F. Le Cras, "Synthèse hydrothermale en continu et en conditions supercritiques du matériau d'électrode  $\text{LiFePO}_4$ ", *Matériaux Congres FFM*, Dion, France, 2006.
2. R. Amin, J. Maier, P. Balaya, D.P. Chen, C.T. Lin, "Ionic and electronic transport in single crystalline  $\text{LiFePO}_4$  grown by optical floating zone technique", *Solid State Ionics*, **179** (2008) 1683–1687.
3. S.-Y. Chung, J.T. Bloking, Y.-M. Chiang, "Electronically conductive phospho-olivines as lithium storage electrodes", *Nat. Mater.*, **1** (2002) 123–128.
4. C.B. Sawyer, C.H. Tower, "Rochelle salt as a dielectric", *Phys. Rev.*, **35** (1930) 269–273.
5. D. Kobor, A.K. Diallo, M. Tine, "Phosphorus based ceramics for positive electrode synthesis and characterization", *J. Modern Phys.*, **5** (2014) 1459–1466.
6. J.T. Evans, Jr., *Application Note AN0701-RTI*, Radiant Technologies, Inc., Albuquerque, USA, 2007.
7. G.Y. Agbéko, "Etude du changement de phase dans le composé  $\text{PbK}_2\text{LiNb}_5\text{O}_{15}$  de la famille des TTB", *Thèse de doctorat en physique*, Université de Toulon et du Var, France, 2002.
8. M.A.L. Nobre, S. Lanfredi, "Thermistor ceramic with negative temperature coefficient based on  $\text{Zn}_7\text{Sb}_2\text{O}_{12}$ : An inverse spinel-type phase", *Appl. Phys. Lett.*, **81** [3] (2002) 451–453.
9. S. Lanfredi, M.A.L. Nobre, "Conductivity mechanism analysis at high temperature in bismuth titanate: A single crystal with sillenite-type structure", *Appl. Phys. Lett.*, **86** (2005) 081916.
10. M.A.L. Nobre, S. Lanfredi, "Negative temperature coefficient thermistor based on  $\text{Bi}_3\text{Zn}_2\text{Sb}_3\text{O}_{14}$  ceramic: an oxide semiconductor at high temperature", *Appl. Phys. Lett.*, **82** [14] (2005) 2284–2286.
11. D. Kobor, B. Guiffard, L. Lebrun, A. Hajjaji, D. Guyomar, "Oxygen vacancies effect on ionic conductivity and relaxation phenomenon in undoped and Mn doped PZN-4.5PT single crystals", *J. Phys. D: Appl. Phys.*, **40** (2007) 2920–2926.
12. M.D. Johannes, K. Hoang, J.L. Allen, K. Gaskell, "Hole polaron formation and migration in olive phosphate materials", *Phys. Rev. B*, **85** (2012) 115106.
13. S.R. Elliott, "A.C. conduction in amorphous chalcogenide and pnictide semiconductors", *Adv. Phys.*, **36** (1987) 135–218.
14. I.G. Austin, N.F. Mott, "Polarons in crystalline and non-crystalline materials", *Adv. Phys.*, **18** [71] (1969) 41–102.
15. R.H. Chin, R.Y. Chang, C.S. Shern, T. Fukami,

- “Structural phase transition, ionic conductivity and dielectric investigations in  $K_3H(SO_4)_2$  single crystals”, *J. Phys. Chem. Sol.*, **64** (2003) 553–563.
16. Y.W. Hong, J.H. Kim, “The electrical properties of  $Mn_3O_4$ -doped ZnO”, *Ceram. Int.*, **30** [7] (2004) 1301–1306.
  17. Y.W. Hong, J.H. Kim, “Impedance and admittance spectroscopy of  $Mn_3O_4$ -doped ZnO incorporated with  $Sb_2O_3$  and  $Bi_2O_3$ ”, *Ceram. Int.*, **30** [7] (2004) 1307–1311.
  18. S. Li, P. Cheng, J. Li, L. Zhao, *Proceedings of the IEEE International Conference on Solid Dielectric, ICSD* (2007) 207–210.
  19. A.F. Kohan, G. Ceder, D. Morgan, C.G. Vande Walle, “First-principles study of native point defects in ZnO”, *Phys. Rev. B*, **61** (2000) 15019–15027.
  20. J. Tellier, Ph. Boullay, D.B. Jennet, D. Mercurio, “Structural versus relaxor properties in Aurivillius type of compounds”, *J. Eur. Ceram. Soc.*, **27** (2007) 3687–3690.
  21. B.J. Kennedy, Y. Kubota, B.A. Hunter, Ismunandar, K. Kato, “Structural phase transition in the layered Bismuth oxide  $BaBi_4Ti_4O_{15}$ ”, *Solid State Commun.*, **126** (2003) 653–658.
  22. T. Badapanda, R.K. Harichandan, S.S. Nayak, A. Mishra, S. Anwar, “Frequency and temperature dependence behaviour of impedance, modulus and conductivity of  $BaBi_4Ti_4O_{15}$  Aurivillius ceramic”, *Process. Appl. Ceram.*, **8** [3] (2014) 145–153.
  23. S. Kumar, K.B.R. Varma, “Relaxor behavior of  $BaBi_4Ti_3Fe_{0.5}Nb_{0.5}O_{15}$  ceramics”, *Solid State Commun.*, **147** (2008) 457–460.
  24. K.S. Cole, R.H. Cole, “Dispersion and absorption in dielectrics I: Alternating current characteristics”, *J. Chem. Phys.*, **9** (1941) 341–351.
  25. V.M. Duda, A.I. Baranov, A.S. Ermakov, R.C.T. Slade, “Influence of the defect structure on the electrical conductivity of  $Pb_5Ge_3O_{11}$  single crystals at high temperatures”, *Phys. Solid State*, **48** [1] (2006) 63–67.

